Journal of Volcanology and Geothermal Research 434 (2023) 107753

Contents lists available at ScienceDirect

Journal of Volcanology and Geothermal Research

journal homepage: www.journals.elsevier.com/journal-of-volcanology-and-geothermal-research

Monitoring of Indonesian volcanoes with the IS06 infrasound array

Duccio Gheri [a,*], Emanuele Marchetti [a], Giacomo Belli [a], Alexis Le Pichon [b], Vincent Boulenger [b], Patrick Hupe [c], Lars Ceranna [c], Pierrick Mialle [d], Philippe Hereil [e]

[a] Department of Earth Sciences, University of Florence, Via La Pira 4, 50126 Florence, Italy
[b] CEA, DAM, DIF, Arpajon, F91297 Paris, France
[c] BGR, Hannover, Germany
[d] CTBTO, Vienna, Austria
[e] VAAC, Meteo France, Toulouse, France

ARTICLE INFO

Keywords:
Infrasonic waves
Early-warning system
IMS
Remote Sensing
Infrasound detection algorithm

ABSTRACT

Detecting and notifying ongoing volcanic explosive eruptions is crucial in supporting the Volcanic Ash Advisory Centre (VAAC). However, local monitoring systems are missing at many active volcanoes, but long range infrasound monitoring might provide useful information if able to detect and notify volcanic explosive events. Indeed, many studies have already highlighted the utility and the potential of long-range infrasound monitoring for this aim, but still open questions remain concerning its actual efficiency and reliability. In this study we investigate the potential of the IS06 array (Cocos Island, Australia) of the International Monitoring System (IMS) of the Comprehensive Nuclear-Test-Ban Treaty Organization (CTBTO) to remotely detect volcanic explosive eruptions in the Indonesian Arc between 2012 and 2019, when 11 volcanoes, positioned at a distance between 1000 and 2000 km from the array, erupted with an energy spanning from mild explosions to VEI (Volcanic Explosivity Index) 4 eruptions. For each volcano, using infrasonic data recorded at a single array and accounting for realistic infrasound propagation conditions, we calculate a range corrected Infrasound Parameter (*IP*) and propose two additional empirical thresholds on signal strength and persistency. The *IP* is used eventually to define an alert whenever an established threshold is exceeded and the corresponding reliability estimated. Results show that the range corrected *IP* is highly reliable for events VEI $= 3$ or greater under favorable propagation conditions, but smaller scale short-lasting explosive eruptions still remain usually undetected. Unresolved ambiguity remains due to short spacing among volcanoes with respect to the array. For regional scale monitoring purposes, this can be solved only considering volcanic sectors rather than single volcanic edifices that, despite preventing unambiguous notification of a given volcano, might allow to increase the attention of the VAAC over a specific area.

1. Introduction

Air transport plays an essential role in the social and economic development of our society. According to International Civil Aviation Organization's (ICAO) annual global statistics, air traffic has been increasing constantly during the last decades reaching a total of 4.5 billion passengers and 38.3 million departures (one every 1.2 s) in 2019 and up to 400 departures of air cargos each hour (ICAO, 2019). Industry estimates prior to COVID-19 suggested a further tripling between 2020 and 2050 (Gössling and Humpe, 2020). The increase in the number of flights reflects an increased probability for aircraft to encounter a volcanic cloud. In the last fifty years, ash clouds produced by 40 volcanoes have damaged aircraft after an encounter (Lechner et al., 2017). Damages might lead to the engine shutdown, due to the high temperature within the turbines that determines ash melting and abrasion (Casadevall, 1994). The majority of encounters occurred for small scale eruptions with Volcanic Explosivity Index (*VEI*)=3 (Guffanti et al., 2010; Newhall and Self, 1982), typically injecting >0.1 km^3 of ash up to an elevation between 3 and 15 km.

As a consequence of the increased hazard related to the volcanic ash encounters, in 1990, the ICAO established the Volcanic Ash Advisory Centre (VAAC), in order to mitigate the impact of volcanic eruptions on commercial flights (Evans, 1994). In case of a volcanic eruption, VAACs collect all available information from volcano observatories,

* Corresponding author.
E-mail address: duccio.gheri@unifi.it (D. Gheri).

https://doi.org/10.1016/j.jvolgeores.2023.107753
Received 30 September 2022; Received in revised form 12 January 2023; Accepted 14 January 2023
Available online 21 January 2023

meteorological offices, satellites images and pilots in order to issue a Volcanic Ash Advisory (VAA) message to aviation users. The VAA consists of a series of information on volcano unrest (e.g. plume height) as well as current plume extent and forecasts.

The physical conditions at an eruptive vent are challenging to be inferred, especially when volcanoes are poorly monitored or observed through satellite-based methods only, which may be limited, e.g., by meteorological cloud cover (Webley and Mastin, 2009), or too sparse in time. Explosive eruptions involve a pressure release by the injection of pressurized gas and material in the atmosphere, generating perturbations as infrasonic waves (Fee and Matoza, 2013; Johnson and Ripepe, 2011). Infrasonic waves can propagate hundreds to thousands of kilometers in atmospheric waveguides (Drob et al., 2003), offering the possibility of performing long-range observations also for those volcanoes located in remote regions. Despite the fact that infrasound propagation is affected by atmospheric specification (e.g. seasonal winds) along the source-to-receiver path, several studies have shown that it is possible to detect volcanic eruptions at large distances (>1000 km) through the use of arrays (Fee et al., 2010; Matoza et al., 2011; De Angelis et al., 2012; Marchetti et al., 2019), thus opening a new perspective in volcano monitoring.

The infrasound network of the International Monitoring System (IMS) of the Comprehensive nuclear-Test-Ban Treaty Organization (CTBTO) monitors the whole geosphere to detect illegal nuclear explosions (Kalinowski and Mialle, 2021) and offers a unique opportunity to provide continuous relevant information about large volcanic eruptions in near real time. Out of the planned network of 60 infrasound arrays, which is designed to detect and locate signals from atmospheric nuclear tests with an equivalent yield of 1*kt* of TNT anywhere on the planet with at least two stations (Pichon et al., 2009; Marty, 2019), 53 certified infrasonic arrays have been deployed during the last 20 years. Since then, several studies highlighted potentials of the IMS infrasound network for studying, among other natural phenomena, explosive volcanic eruptions (Dabrowa et al., 2011; Matoza et al., 2011; De Angelis et al., 2012; Fee and Matoza, 2013; Caudron et al., 2015; Marchetti et al., 2019; Perttu et al., 2020; Pichon et al., 2021), suggesting that long range infrasound might be of great support to the VAACs, being able to provide timely information of ongoing events. Steps towards this goal have been taken by considering both single or multiple arrays approaches. Matoza et al. (2017) proposed a brute-force, grid-search, cross-bearing method to identify explosive volcanic eruptions from the IMS infrasound bulletin that has proved to be able to detect automatically three out of the seven VEI 4 eruptions that occurred globally between 2005 and 2010. On the other end, considering a 2.5 year-long period, Marchetti et al. (2019) demonstrated how the Etna volcano could be monitored by a single station located at 1040 km with a reliability of 87 % during favourable atmospheric propagation. Nevertheless, a systematic analysis on the real efficiency of the IMS infrasound network to automatically detect volcanic eruptions at large distances is still missing and further analysis is required to estimate the confidence level and the number of false alerts.

In this work, we evaluate the capability of detecting volcanic eruptions through one station of IMS infrasound network and provide the reliability on the notifications. We apply a method based on the infrasound parameter (*IP*) defined originally for local infrasound array data by Ulivieri et al. (2013) and Ripepe et al. (2018) as a fully automated early warning system for Etna volcano. Following the work of Marchetti et al. (2019), we extend such procedure to regional and global observations and define warning notification thresholds according to source-to-receiver distances and accounting for propagation effects. We focus initially on infrasound produced by the December 2018 Anak-Krakatau eruption recorded by IS06 array, at a distance of 1155 km, in order to refine and consolidate the simple procedure of long-range infrasound monitoring that was already successfully applied to Etna (Marchetti et al., 2019) and Stromboli (Pichon et al., 2021) volcanoes. Then, we extend the procedure to all Indonesian volcanoes within a maximum distance of 2000 km from the station focusing only on volcanoes which erupted in the last decade (2012–2019) according to Engwell et al. (2021) and bulletin reports of the Global Volcanism Program (GVP). Such comparison is used to define the efficiency of the IS06 IMS infrasonic array to monitor the selected volcanoes with this new approach. A robust and quantitative analysis of the false alert rate is presented and discussed.

2. Data

In this study we consider infrasound data recorded during an eight year-long period (2012–2019) by the infrasound array IS06 of the IMS network of the CTBTO, deployed on Cocos Island, south of Sumatra (Fig. 1a and 2ab). IMS infrasound data are microbarometric array data recorded continuously at the sampling rate of 20 Hz. IMS infrasound arrays have an aperture between 1 and 2 km (Christie and Campus, 2010), optimized for the 0.1–1 Hz frequency band (Marty, 2019), and are typically deployed in quiet environments. Each microbarometer array element has a flat and stable response within ~ 5% in amplitude over the 0.02–4 Hz frequency band and is equipped with a "pipe array" wind noise reduction system (Marty et al., 2017) that allows increasing signal-to-noise ratio and reaching measurable signals as low as 1 mPa (Bowman et al., 2005). The IS06 array consists of 8 array elements, with an aperture of 2 km (Fig. 2b), and is equipped with MB2000 microbarometers. The array has been deployed in 2010 and eventually certified in 2012. Since then, the array is sending data to Vienna in real time with a sampling rate of 20 Hz.

We focus on active volcanoes positioned around the array and within a source-to-receiver distance <2000 km (Fig. 1a,b). This limit was chosen because, although major volcanic eruptions have been recorded by infrasound arrays at greater distances (Dabrowa et al., 2011), the large travel time exceeding 110 min would strongly limit its application as warning system. Based on these geometrical constraints, 64 volcanoes that showed activity in the Holocene (Venzke, 2013) can be identified from the catalogue of the GVP. Of these, 11 volcanoes were active in the period of interest (Fig. 1a,b). The active volcanoes were identified reviewing the GVP reports and list of VAAs issued for all the volcanoes of the world as reported in Engwell et al. (2021).

According to GVP reports, in the period 2012–2019 four VEI⩾3 eruptions occurred at Anak-Krakatau, Sinabung and Kelut volcanoes, while lower energy explosive activity resulting in small ash plumes, ash puffing, and steam plumes and lava flows were reported for the volcanoes Marapi, Kerinci, Dempo, Slamet, Merapi, Tengger Caldera, Semeru, and Raung. The main volcanic activity is summarized in Table 1.

Since June 2018, Strombolian and Vulcanian activity at Anak-Krakatau, located at 1155 km with a back-azimuth of 55°N was tracked by MODIS (MODerate resolution Imaging Spectroradiometer) (Walter et al., 2019), leading to a volcanic radiative power (VRP) of around 100 times larger than long term thermal emission from the volcano. Such a persistent activity increased from August to November and led to a massive ($\approx 25.5 \pm 8.4$ Mm^3) accumulation of newly erupted material on the eruptive cone (Walter et al., 2019). The activity culminated on December 22, 2018 with a sector collapse followed by a catastrophic tsunami and explosions producing a 12–16 km high ash plume (Walter et al., 2019; Grilli et al., 2019; Perttu et al., 2020; Ye et al., 2020; Rose and Matoza, 2021). After the collapse, the transition to explosive Surtseyan style eruptions with >10 km high plumes occurred until January (Perttu et al., 2020). This eruptive phase was classified as VEI 3 (Venzke, 2013).

Kelut volcano, positioned at 1750 km from the array and with a back-azimuth of 75° N, experienced a major VEI 4 eruption in February 2014 (Venzke, 2013) that caused the disruption of the dome which plugged the conduit and produced an ash plume which rose up to 26 km (Kristiansen et al., 2015), reaching the stratosphere. The event radiated high amplitude, long-lasting atmospheric acoustic waves that were recorded

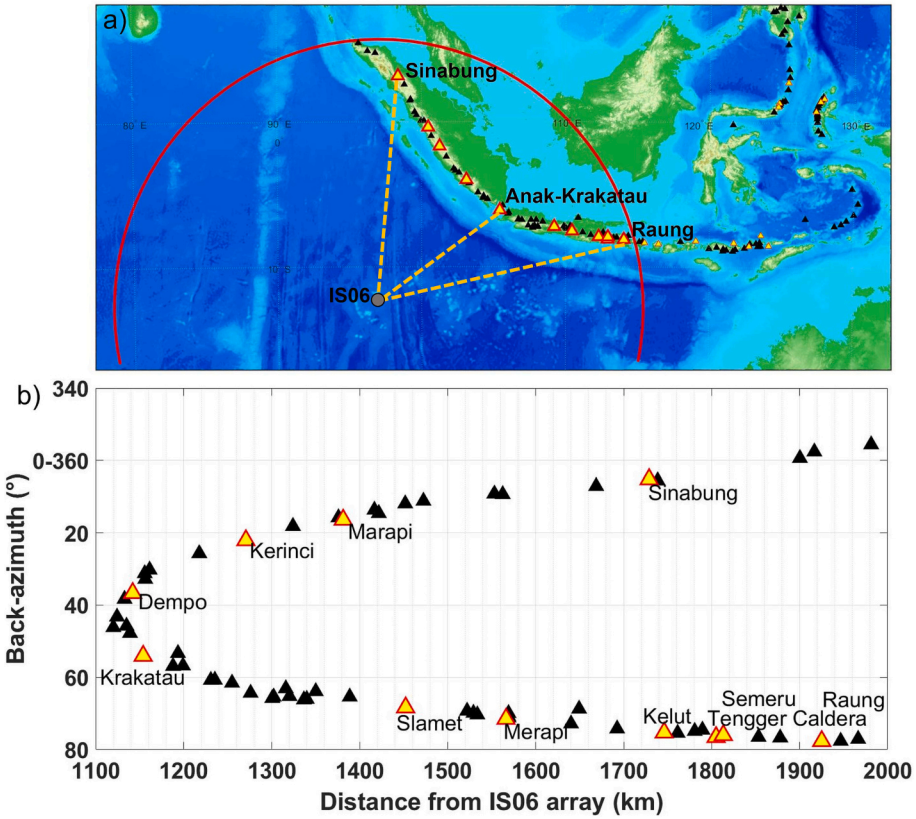

Fig. 1. Location of volcanoes in Indonesia (triangles) within a source-to-receiver distance <2000 km from the IS06 IMS infrasound array (grey dot) deployed on Cocos Island in the Indian Ocean. Volcanoes that were active during the Holocene (Venzke, 2013) are colored in black, while yellow triangles represents volcanoes that had activity during the last decade (*a*, *b*). In *a*, the three dashed yellow lines point to Sinabung, Anak-Krakatau and Kelut volcanoes, positioned (*b*) at distances of 1720, 1155 and 1750 km from IS06 infrasound array respectively and correspond to back-azimuth values of 5, 55 and 77 ° N.

as far as 11000 km from the source (Caudron et al., 2015).

During the period of analysis, Sinabung volcano, positioned at 1720 km from the array and with a back-azimuth of 5° N, was characterized by two long lasting eruptive cycles, both classified as VEI 4 events. The first one started on September 2013 and lasted five years generating a series of phreato-magmatic explosions, lava dome collapses with pyroclastic flows and frequent ash plumes <7 km a.s.l. (Gunawan et al., 2019). According to GVP reports, the eruption climaxed on the 19 February 2018 with the explosion of the dome which produced a 17 km high eruptive column. The second eruptive cycle took place during February-June 2019, with the main events observed on 24 May and 9 June 2019, leading to plumes reaching 15 km altitude.

3. Methods

For evaluating the infrasound detection capability of the IMS infrasound network and estimate the rate of false alerts, we apply a procedure based on the infrasound parameter (*IP*) (Ulivieri et al., 2013; Ripepe et al., 2018; Marchetti et al., 2019). The procedure adopted here consists of four steps: 1) array processing of infrasound data, 2) correction for propagation effects, 3) estimating the *IP*, 4) warning notification and reliability.

In order to calibrate the algorithm, we first analyzed infrasound data of the December 2018 Anak-Krakatau eruption recorded by the IS06 infrasound array (Fig. 3a), being the station conveniently located with respect to the Indonesian Arc (Fig. 1a). Eventually, to test the procedure and evaluate its reliability, we extended the analysis to infrasound data recorded between the beginning of 2012, when the station was certified and started providing data to Vienna, and December 2019 (Sections 4.1 and 4.2).

3.1. Array processing

We use the array data to estimate wavefront parameters of coherent infrasound plane waves using correlation time delays between array element triplets. As a result, we identify detections whenever coherent infrasound signal is recorded across the array over the time window of analysis, allowing to fully characterize the recorded infrasound wavefield. As shown in Fig. 2c, detections obtained from a multi-spectral analysis fully characterize infrasound recorded at IS06 array in terms of preferential propagation directions (e.g. East and Southwest) and spectral content, and suggest coexistence of multiple sources of infrasound energy around the array. Concerning infrasound from Indonesian volcanoes, we expect that signal recorded at IS06 array is dominated by stratospheric arrivals, whose peak frequency content is typically expected around 2 Hz (Pichon et al., 2012). Indeed, infrasound detections of volcanic origin show a frequency content slightly above 1 Hz (see also Rose and Matoza (2021)), differently from other sources (e.g. microbarom) that dominate the background wave-field with similar back-azimuth but with a lower frequency content (Fig. 2c). For these reason, a specific array processing in the 1–3 Hz frequency band was applied by using a multichannel correlation analysis in the time domain over 60-s-long moving time windows (*w*) and with a time shift (*dt*) of 10 s. Fig. 3 shows the resulting detections, which describe the recorded infrasound wave-field in terms of pressure amplitude (Fig. 3b), back-azimuth (Fig. 3c), and apparent velocity (c_a, Fig. 3d). While back-azimuth, being defined from the receiver to the source, directly identifies the direction of infrasound propagation (i.e. the direction from where the signal is coming from), apparent velocity relates to sound propagation velocity (c) by accounting the wave incidence angle (γ), according to:

$$c_a = \frac{c}{sin(\gamma)} \quad (1)$$

and is thus representative of the infrasound ray-path and/or source altitude in the atmosphere.

Fig. 3a shows 1–3 Hz band-pass filtered infrasound data recorded between December 16 and December 31, 2018, by 7 elements of the IS06

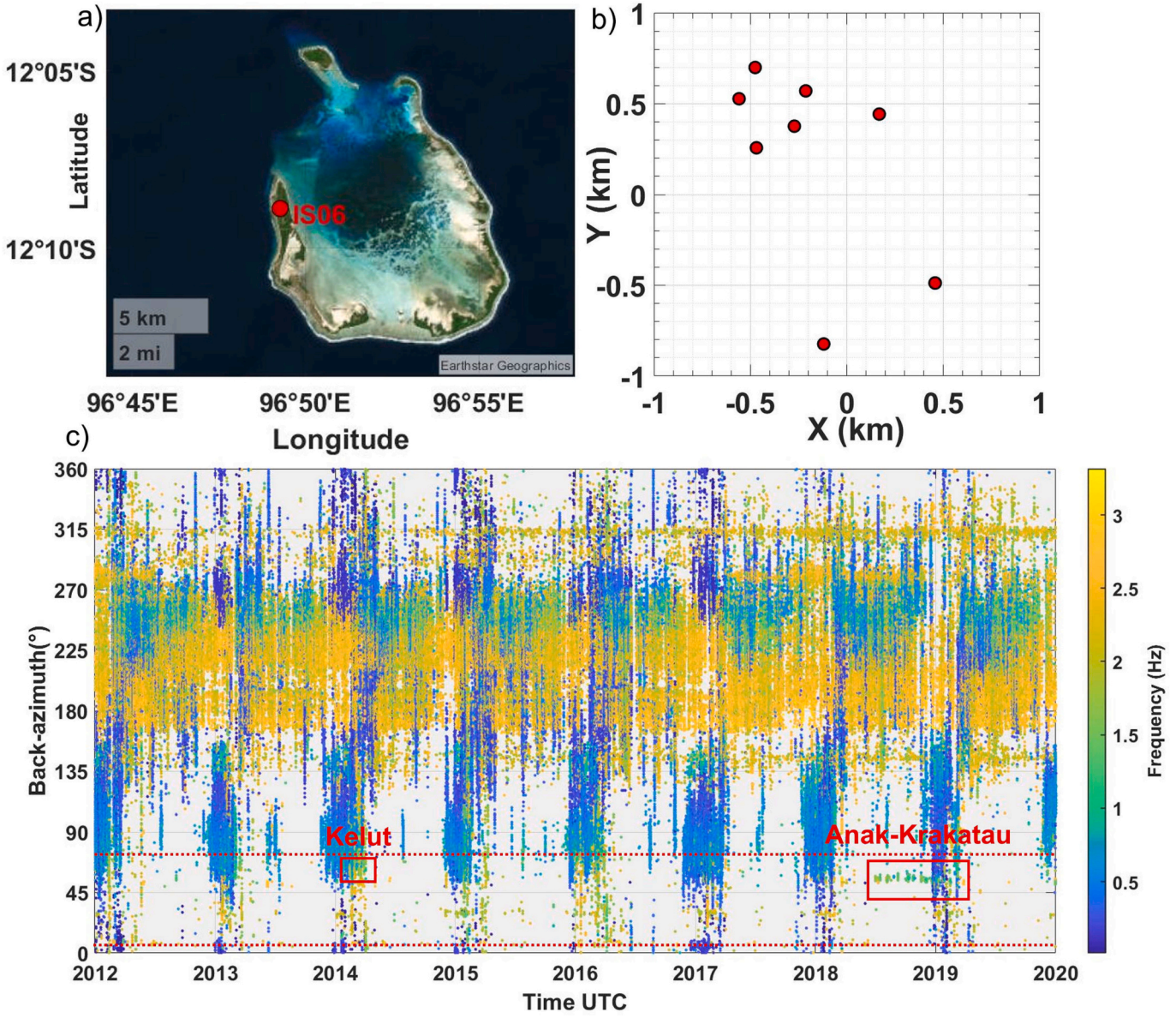

Fig. 2. Cocos Island archipelago with the position of IS06 infrasonic station, while in *b*, the array geometry is depicted. In *c*, the detections obtained from the Progressive Multichannel Correlation (PMCC, Cansi, 1995) array processing, are shown in term of back-azimuth (y-axis) and frequency (colorbar). The red dashed lines represent the azimuth range within fall Indonesian volcanoes with respect to the array. The eruptive activity of Kelut and Anak-Krakatoa are enclosed within the red box.

array (one element did not work). From the morning of December 22, coherent infrasound was recorded with a back-azimuth of 54°N (Fig. 3c) pointing to Anak-Krakatau volcano, that is positioned at a distance of 1155 km from the array (Fig. 1c). The recorded amplitude at the array increased rapidly in the morning of Dec. 22 to reach a peak of 0.12 Pa around 11:54:05 UTC, and decreased shortly before the paroxysmal phase ended and the flank collapse occurred at 13:55:49 UTC (Fig. 3b). Infrasound with a back-azimuth consistent with Anak-Krakatau (Fig. 3c) continued to be recorded until the end of 2018, indicating the persistency of explosive activity at the volcano. Despite some gaps in the detections, likely due to the low signal-to-noise ratio produced by local wind effects, back-azimuth and apparent velocity (Fig. 3c,d) were quite stable during the eruption, suggesting stable propagation conditions between the volcano and the IS06 array. On the contrary, peak amplitude at the array (Fig. 3b) shows variations, with clear discrete peaks recorded mostly after December 26. These amplitude variations might reflect source strength as well as propagation effects between the source and the receiver.

3.2. *Infrasound propagation*

Long-range (>200 km) infrasound observation is strongly affected by atmospheric propagation effects (Drob et al., 2003). Here, infrasound ducting is most efficient within the stratospheric waveguide, between the ground and the stratopause, and leads typically to infrasound detections with a frequency content peaking between 1–3 Hz. Lower frequency (<1 Hz) infrasound is also commonly recorded for thermospheric arrivals, as a consequence of the larger atmospheric rarefaction at high altitude, resulting in stronger attenuation of higher frequencies of infrasonic waves.

Following Pichon et al. (2012) We calculate atmospheric attenuation (A_P) of infrasound waves as a function of signal frequency (f) and the effective sound speed ratio ($V_{eff-ratio}$), from the empirical equation:

Table 1
Reported activity of the eleven Indonesian Volcanoes active in the period of analysis 2012–2019.

Indonesian active volcanoes	Reported activity
Sinabung	Phreatomagmatic explosions, lava dome collapses, pyroclastic flows and continuous ash plumes. Main events occurred in February 2018 May-June 2019.
Marapi	Short-lived phreatomagmatic explosions with ash plume on November 2015, June 2017, April/May 2018 <7 km a.s.l..
Kerinci	Intermittent explosions, ash plumes (maximum height 6.7 km a.s.l.), and gas-and-steam plumes especially on 2016, 2018 and 2019.
Dempo	Low-energy phreatic explosions at the crater lake on December 2017.
Krakatau	High-intense Strombolian/Vulcanian activity until December 22 (2018), then Surtseyan activity.
Slamet	Low-intense Strombolian activity, with weak and sporadic ash plumes, lava flows and steam plumes in the period between March and September 2015.
Merapi	Continuous lava dome extrusion after the October 2010 Vulcanian activity. The partial disruptions of the new dome cause low level ash plumes throughout the analysed period.
Kelut	On February 2014, the disruption of the dome causes a Plinian eruption with an ash plume up to 26 km.
Tengger Caldera	Frequent weak ash emission (<7 km a.s.l.). Main eruptive event occurred on December 2015, July 2016, February-July 2019.
Semeru	Dome growth and regular ash plumes (<4.5 km a.s.l., February-August 2018), with pyroclastic flows (February-April 2012, February-July 2015), rock-avalanches (August 2015), and frequent lava flows.
Raung	The main intense activity occurred on 2015 with an ash plume periodically reaching a maximum height of 9 km a.s.l..

$$A_P(f, V_{eff-ratio}) = \frac{1}{R}10^{\frac{\alpha(f)R}{20}} + \frac{R^{\beta(f,V_{eff-ratio})}}{1+10^{\frac{\delta-R}{\sigma(f)}}} \quad (2)$$

where R is the source-to-receiver distance, α, β, δ and σ are parameters derived from multidimensional curve-fitting of parabolic equation simulations while $V_{eff-ratio}$ is the ratio between the effective sound speed (adiabatic speed of sound summed to the wind component in the propagation direction) at an altitude of 50 km to the speed of sound at sea level. The first term of Eq. (2) describes the attenuation of the direct wave by geometrical spreading and exponential decay (α). The second term describes the attenuation in the acoustic duct, with β being the transmission loss accounting for the geometrical spreading and dissipation of stratospheric and thermospheric waves, while δ is the width of the shadow zone (i.e. where stratospheric arrivals are not expected at the ground) and σ is a scaling distance controlling the attenuation in the shadow zone.

Fig. 4a shows the $V_{eff-ratio}$ and A_P for a 1-year-long period between June 2018 and June 2019. The $V_{eff-ratio}$ was calculated considering a daily atmospheric profile above the volcano calculated up to a height of $\sim$ 60 km from ERA-Interim (horizontal resolution of 1°, 60 vertical levels) and ERA5 (horizontal resolution of 0.25°, 37 vertical levels) data provided by the European Centre for Medium-Range Weather Forecasts (ECMWF). The A_P is calculated considering the source-to-receiver distance (R) of 1155 km, a frequency of 2 Hz, in agreement with the band-pass frequencies (1–3 Hz) applied for array processing as discussed in Section 3.1 and assuming constant propagation conditions between Anak-Krakatau and IS06 array. The $V_{eff-ratio}$ shows a clear variation during the year, with downwind propagation conditions ($V_{eff-ratio}$ >1) observed between November and April and upwind ($V_{eff-ratio}$ <1) conditions occurring during the Austral winter, that is controlling the attenuation of infrasound wave propagation. In December 2018, a low attenuation of −55 dB related to $V_{eff-ratio}$=1.1 is ensuring an efficient propagation that is resulting into a clear detection of infrasound produced by the Anak-Krakatau eruption at the distal array (Fig. 3b).

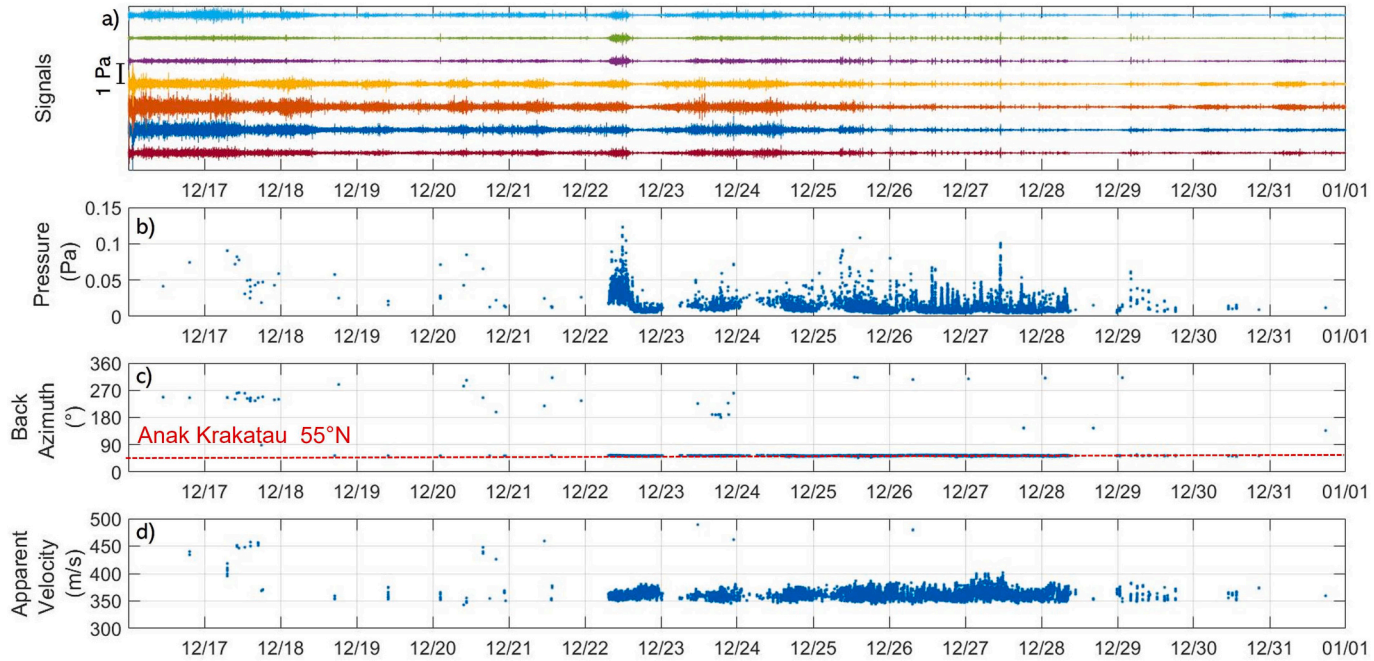

Fig. 3. 23 days of infrasound data recorded by 7 elements of the IS06 IMS array showing the December, 2018, explosive eruption of Anak-Krakatau volcano. a) 1–3 Hz bandpass filtered waveforms, b) amplitude (Pa), c) back-azimuth (°N) and d) apparent velocity (m/s) of infrasound detections obtained from correlation analysis on 1–3 Hz band-pass filtered data.

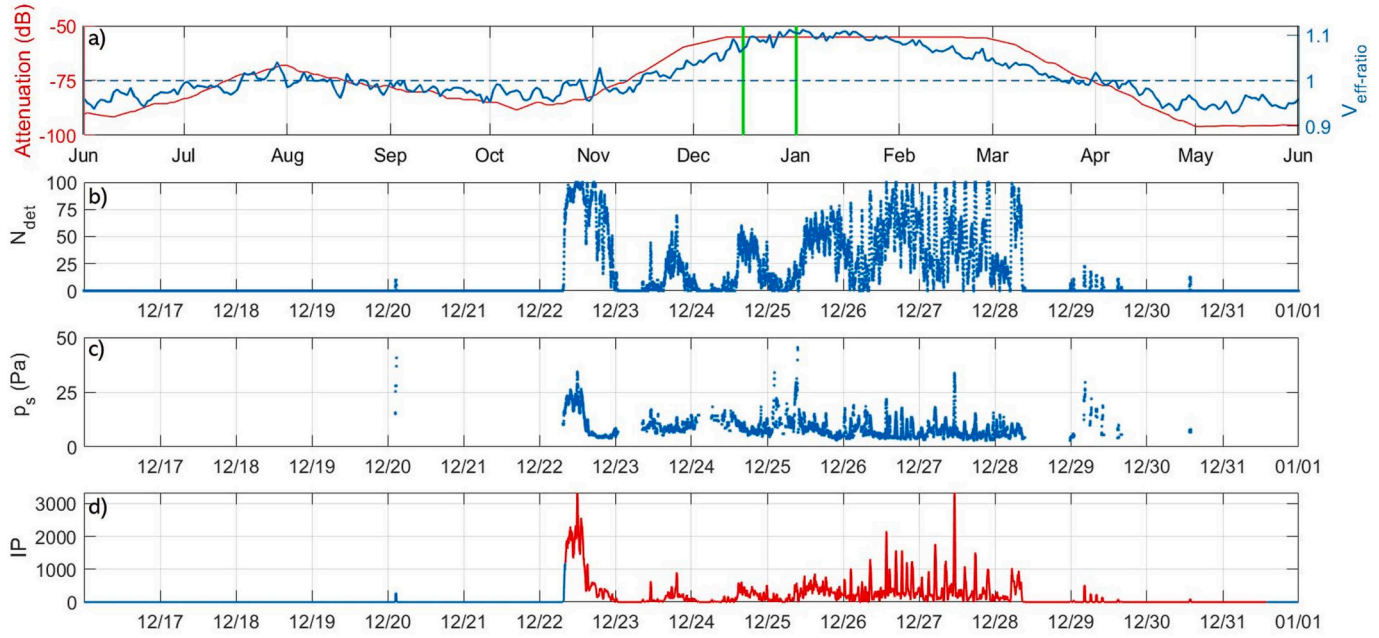

Fig. 4. $V_{eff-ratio}$ (blue) between Anak-Krakatau and IS06 array and corresponding A_P (red) calculated for a peak infrasound frequency of 2 Hz between June 2018 and June 2019 (a). Refraction of energy in the stratopause region towards the ground is predicted when $V_{eff-ratio}$ >1 (downwind propagation), corresponding to low attenuation (−50/−75 dB) of infrasound radiated from Anak-Krakatau and recorded at IS06 array. High attenuation (<−75 dB) is predicted for upwind propagation ($V_{eff-ratio}$ <1). The vertical green lines correspond to the main eruptive phase of Anak-Krakatau, that started on 22 December 2018 as shown in the lower panels. The number of detections, N_{det}, reflects the persistency of the signals (b). Mean infrasonic pressure retrieved at the source, p_s (c). *IP* (d) calculated every minute for Anak-Krakatau from infrasound records from IS06 array at the source-to-receiver distance of 1155 km considering a time window (*W*) of 20 min. The *IP* is colored in red when exceeding the threshold value defined in Section 3.4.

3.3. The Infrasound Parameter (IP) from long-range observation

In order to evaluate the strength and persistency of infrasound energy radiated by the volcanic eruption of Anak-Krakatau recorded at IS06 array, we compute the Infrasound Parameter (*IP*) defined as:

$$IP = n_{det} \times p_a, \tag{3}$$

where n_{det} is the number of infrasound detections and p_a is the mean infrasonic pressure both recorded at the array in a given time window.

By applying such procedure to long-range infrasound detections we follow Marchetti et al. (2019) and limit the analysis to detections with a measured back-azimuth B_{az} that is consistent with the back-azimuth corresponding to the volcano (az_V) and allowing a deviation (Δaz_V) of ±3°. This latter is required to account for the azimuthal deviation of the acoustic source-to-receiver ray-path induced by propagation effect (e.g. winds) (Pichon et al., 2005) at the time of the event. Moreover, consistently with the calibration performed on eruptive activity from Etna volcano recorded at source-to-receiver distances exceeding 500 km (Marchetti et al., 2019), we normalize the number of detections to account for long range propagation and correct infrasound pressure recorded at the array for the attenuation expected accounting for the actual atmosphere specification.

The normalized, range independent, number of detections (N_{det}, Fig. 2b) is defined according to:

$$N_{det} = \frac{n_{det} dt}{W} \times 100, \tag{4}$$

where *dt* is the time shift applied for correlation analysis and n_{det} is the number of detections with an infrasound back-azimuth consistent with the volcano in the time window of analysis (*W*). The *W* is related to the source-to-receiver distance in order to account for increasing signal duration with distance as a result of multiple raypaths. In particular, *W* = 5 min is used for *R* <500 km, *W* = 10 min for 500 km <*R* <1000 km, and *W* = 20 min for *R* >1000 km. Considering that infrasonic data are processed with a 60-s-long-time window shifted by *dt* = 10 s and that the time window of analysis *W* is fixed to 20 min, n_{det} can reach the maximum value of 120, that would correspond to the range independent, normalized N_{det}=100 according to Eq. (4), when signal from the volcano is recorded persistently at the distant array. As shown in Fig. 4b, N_{det} reaches the peak value only during the December 22 paroxysmal phase of the eruption, then reduces afterwards and reaches the maximum value again during short lasting discrete episodes.

The propagation effects from Anak-Krakatau to IS06 array are accounted for considering the attenuation defined by Eq. (2) and calculated in the period of analysis. Adopting realistic atmosphere, the range corrected amplitude at the reference distance of 1 km from the volcano (p_s) is obtained using infrasound pressure recorded at the array (p_a) with:

$$p_s = \frac{p_a}{A_P}. \tag{5}$$

Fig. 4c shows that p_s exceeded 30 Pa during the paroxysmal phase of December 22 and fluctuated around 10 Pa during the 7 days of persistent activity. Pressures are underestimated as relating to the most energetic phase of the entire eruption (Perttu et al., 2020). This result from the pressures are mediated over a 20-min time window, thus smoothing out all peaks. Moreover, pressure's retrieve at 1 km distance from the source is obtained through the experimental Eq. (2), which does not take into account the an-elastic effects that occur in the first km traveled by the acoustic waves.

Following Eq. (3), the product between N_{det} and p_s is providing an infrasound parameter (*IP*) that is representative for a given volcano independently from the source-to-receiver distance and propagation conditions. The *IP* calculated for Anak-Krakatau with data collected at 1153 km by the IS06 infrasound array (Fig. 4d) shows a rapid increase on December 22, to reach peak values exceeding 1000, and fluctuates afterwards for the following six days. Results clearly show that the *IP* is

strongly affected by the persistency of infrasound signal (N_{det}), that maximizes at the beginning of the eruption on December 22, reduces afterwards and peaks again during transient explosive events starting on December 26, 2018. Both N_{det} and p_s shown in Fig. 4, and consequently the *IP*, are calculated every minute and refer to the previous 20 min-long time interval.

3.4. Infrasound warning from long-range observations

The normalization of the number of detections defined by Eq. (4), and the correction of recorded infrasound pressure defined by Eq. (5), allow to apply the same threshold for long range infrasound observations already adopted by Marchetti et al. (2019) for Etna and by Pichon et al. (2021) for Stromboli volcanoes. We additionally parameterize the time period required for *IP* to exceed the threshold value of 100 to be 3/2 of the time window of analysis (*W*). This corresponds to 30 min for the analysis of Anak-Krakatau, but will vary whenever a different time window is applied.

Application of such an approach to *IP* highlights that a notification of increased volcanic activity at Anak-Krakatau would have been issued at 08:04:00 UTC on December 22, 2018, 6 h before the sector collapse and tsunami, as a consequence of increased persistency of signal detection at the array (Fig. 4b) and and pressure amplitude at the source (Fig. 4c). In agreement with Ripepe et al. (2018) the volcanic activity might be considered back to normal once the *IP*, after the eruptive crisis, remains below 14 for a period of 24 h. With this assumption as a consequence of the persistency of explosive activity at Anak-Krakatau, the warning would have persisted until December 31, 2018 (Fig. 4d).

This analysis corroborates previous studies of long range infrasound observations of volcanic activity and confirms that automatic warning might be delivered for selected eruptive episodes (Matoza et al., 2017; Marchetti et al., 2019; Pichon et al., 2021). However, a systematic analysis of the number of false alerts and an efficiency estimation over a longer time period is still missing. Hence, we quantify the reliability of IS06 infrasound IMS array to monitor Indonesian volcanoes by introducing the Reliability Ratio, R_{rel}, defined as:

$$R_{rel} = \frac{Nra}{N_{TOT}} \times 100, \tag{6}$$

where N_{TOT} is the total number of notifications based on long range infrasound observations from IS06 array, while N_{ra} is the number of notifications really corresponding to increased volcanic activity. For a given volcano, a notification is considered reliable if its timing matches the occurrence of an eruptive event, obtained both from GVP reports (not always clear) and from dedicated available research studies. According to Eq. (6), R_{rel} ranges between 0 and 100; 0 indicates that for the selected volcano we have only false alerts, therefore long range infrasound observation is not reliable for monitoring purposes; 100 corresponds to all notifications being reflective of ongoing volcanic activity, and suggests that the array is conveniently located to monitor the volcano. Eventually, R_{rel} could be undetermined due to the absence of notifications ($N_{TOT} = 0$).

4. Results

4.1. Application to Anak-Krakatau volcano

In order to further examine and test the presented procedure, we extended the analysis for Anak-Krakatau over a longer time period spanning between January 2012 and December 2019 (Fig. 5a). The *IP*, calculated following the procedure described in Sections 3.3 and 3.4, exceeds the threshold 10 times: three times (28 February 2013, 19 March 2014, 22 March 2018, all false alerts) before the onset of the 2018 eruption, six times during the 2018 eruptive crisis, both during the the precursory high-intensity Strombolian activity (04 August 2018, 06 August 2018, 08 October 2018 and 18 November 2018) and during the paroxysmal phase 22 December 2018 and the first of January 2019, and once at the end of 2019, when no eruption was ongoing at the volcano. These results show that the activity at Anak-Krakatau might be monitored successfully from the distal infrasound observation but also that, during the 8-year-long time period of analysis, additional sources of infrasound with a back-azimuth consistent with the volcano occurred, that might have lead to possible false alerts. In particular, we obtain 10 notifications but only 6 of them correspond to increased volcanic activity, thus resulting into a $R_{rel} = 60\%$.

In order to reduce the number of false alerts and increase the reliability of the algorithm, we apply two additional thresholds both on the

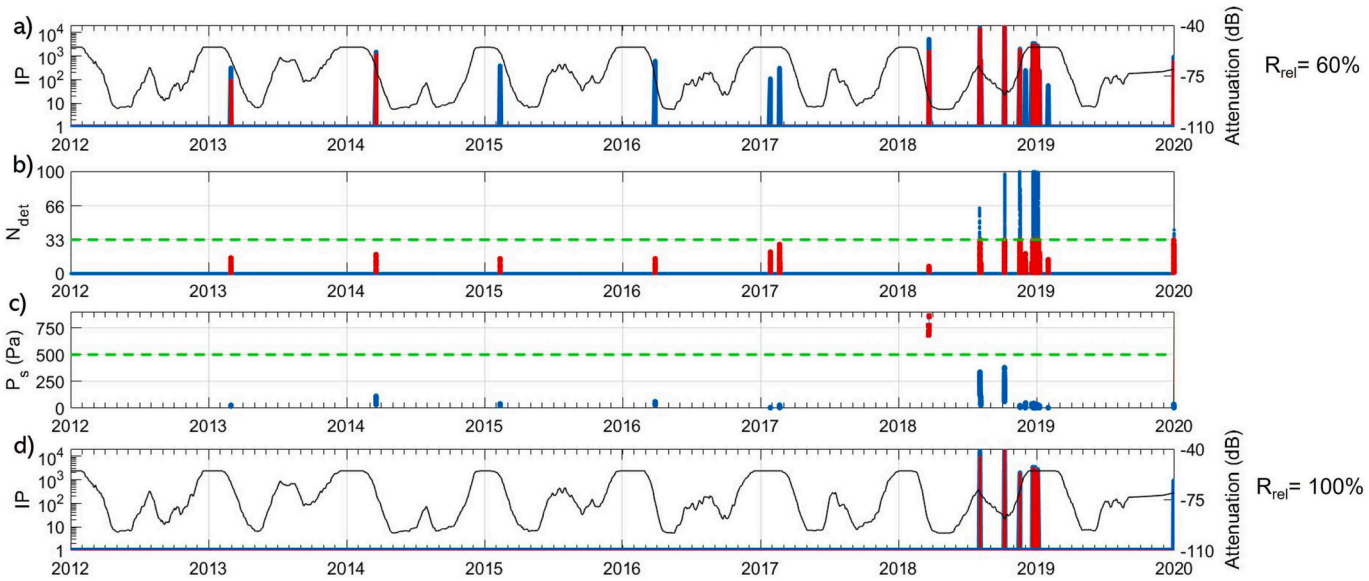

Fig. 5. *IP* calculated for Anak-Krakatau from IS06 array data between January 2012 and December 2019 (a). *IP* is shown with the blue line and, when the warning threshold of 100 is exceeded according to Section (3.4), the *IP* is colored in red. Normalized number of detections, N_{det} (b), and mean infrasound pressure at the source, p_s (c), measured within the time window of analysis (*W*) and used to calculate the range corrected *IP* (a). Data with a normalized number of detections below 33 and/or a mean corrected amplitude at the source exceeding 500 Pa are excluded from the analysis (red). *IP* calculated for Anak-Krakatau after the additional thresholds are applied (d). In subplots a and b, the attenuation (black) is over-imposed to calculated *IP*.

persistency of detections (N_{det}) and on the range corrected pressure at the source (p_s). The majority of the non-volcanic infrasound signals recorded at IS06 array before 2018 are characterized by $N_{det} < 33$ (Fig. 5c), while signal gets more persistent only during the 2018 eruptive phase of Anak-Krakatau. We therefore exclude all signals characterized by low ($N_{det} < 33$) signal persistency, as likely produced by non volcanic sources, or short lasting volcanic events.

Another key aspect of the *IP* calculation is the range corrected pressure (p_s) obtained for Anak-Krakatau from infrasound records at IS06 array. Even during major explosive eruptions, the pressure at the source retrieved from long range observations does not exceed several hundreds of Pa, see Fig. 5c. Therefore we suggest to exclude from the calculation of *IP* all range corrected pressure at the reference distance of 1 km that are exceeding 500 Pa, since they likely represent a source closer to the station instead of a real distant volcanic source. Fig. 5c shows that for Anak-Krakatau, the signal recorded on March 2018, once corrected for propagation effects, is exceeding the p_s threshold of 500 Pa and is therefore not considered as a signal from the volcano.

The *IP* calculated for Anak-Krakatau from distal infrasound records at IS06 array and including the two additional thresholds presented above is shown in Fig. 5d. Here, the amplitude of the *IP* is strongly reduced for non volcanic signals recorded before 2018 and the *IP* is exceeding the threshold of 100 only 5 times, all corresponding to an increased volcanic activity at the source, thus resulting into a $R_{rel} = 100$. All false alerts are indeed removed. By applying the additional thresholds however, the real notification of August 6, 2018, shown in Fig. 5a is removed too, as the recorded infrasound signal is associated to a low persistency ($N_{det} = 10$).

4.2. IP calculated for the Indonesian Arc

During the period between January 2012, when data from IS06 infrasound array were first available, and December 2019, volcanic activity in the Indonesian Arc was quite intense. According to GVP reports and Engwell et al. (2021), 11 out of 64 volcanoes, located at distances between 1142 and 1925 km and with a back-azimuth spanning from 5 to 78°*N* from IS06 array (Fig. 1a,c), had activity with different style and intensity (see Table 1).

Fig. 6 shows the *IP* computed for the 11 recently active volcanoes throughout the period of analysis. The *IP* is colored in red during the time period when the threshold of increased activity (Section 4.1) is exceeded and a notification is expected. For major explosive eruptive events at Anak-Krakatau, discussed in detail in Section 3.4, and the eruption of Kelut volcano on 2014, the *IP* is increasing only during the real eruptive phases (Fig. 6) and and the distal array is efficiently monitoring the volcanic activity without issuing any false alerts ($R_{rel} = 100$).

It is worth noting from Fig. 6 that the *IP* calculated for Merapi (71° N), Tengger Caldera (75° N), Semeru (76° N) and Raung volcano (77° N) is very similar to the one calculated for Kelut volcano (75° N), as a

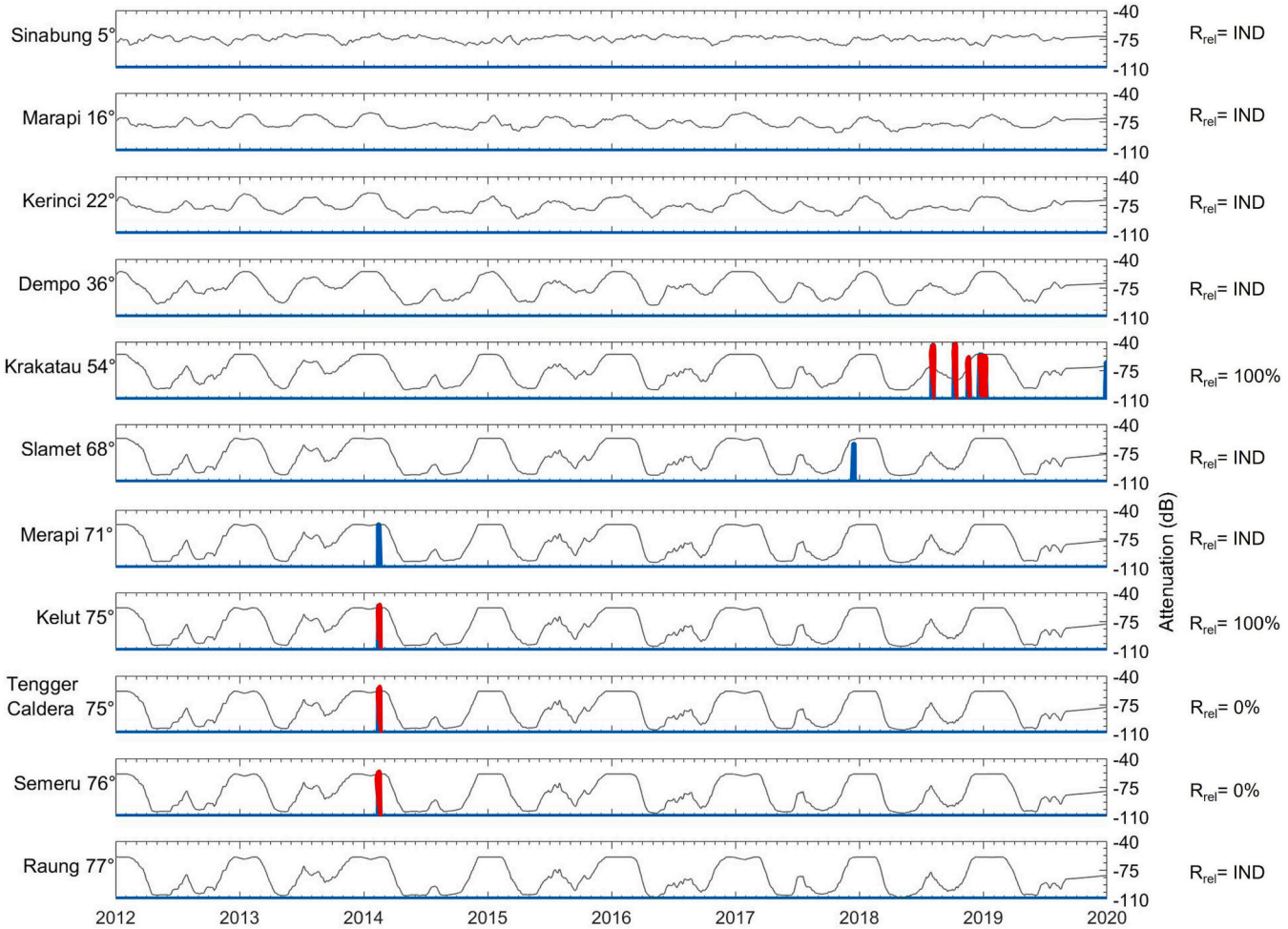

Fig. 6. Infrasound parameter (*IP*, blue line) and Reliability Ratios (R_{rel}) calculated for the 11 Indonesian volcanoes (with the corresponding back-azimuth with respect to station IS06) for whom activity was reported between 2012 and 2019 (Engwell et al., 2021). The *IP* is colored in red when the threshold of 100 is exceeded and a notification is expected. The black line in each subplot represents the attenuation (A_P) calculated from the ECMWF climatological model along the source-to-receiver path (Section 3.2).

consequence of the back-azimuth deviation (Δaz_V of ±3°, see Section 3.3) applied to identify infrasound from a given volcano. Indeed, the strong signal of the February 2014 Kelut eruption determined an increase not only of the *IP* of Kelut volcano, but also of the *IP* of the volcanoes with similar expected back-azimuth. Indeed, once the threshold of increased activity is applied according to Section 3.4, the computed *IP* leads to a false alert for Tengger Caldera and Semeru volcanoes and therefore results into a corresponding R_{rel}=0. For Merapi volcano on the contrary, the increase of the *IP* was too short (21 min) to exceed the notification threshold.

For the other volcanoes, in accordance to the low level of activity reported (Table 1), the *IP* calculated from long range infrasound data recorded at IS06 array remains low and notifications are not expected. This was the case also for the Sinabung, despite being associated to a much stronger (VEI = 4) activity. The lack of notification prevents us from evaluating the efficiency of the distal infrasound observation to detect and monitor volcanic activity from these volcanoes.

5. Discussion

Results presented in this study demonstrate that long-range (>1000 km) infrasound array observations are usable to detect and notify high intensity (VEI ⩾3) volcanic eruptions with a good reliability during favorable atmospheric propagation of infrasonic waves. The 2018 Anak-Krakatau and the 2014 Kelut explosive eruptions, that both occurred during favorable westward infrasound propagation towards Cocos Island, are well detected by IS06 array, at a source to receiver distance exceeding 1000 km, and the recorded signal could be used to provide an automatic alert. However, in order to increase the system reliability, starting from the early-warning of explosive eruptions originally developed by Ripepe et al. (2018), and adapted by Marchetti et al. (2019) to long range observations, we propose two additional experimental thresholds on range corrected amplitude ($p_s < 500Pa$) and persistency of the detections ($N_{det} > 33$) to minimize false alerts.

Although a low signal-to-noise ratio, as shown for the Anak-Krakatau eruption (Fig. 3) prevents the coherent infrasonic signals of ongoing eruptions, the proposed algorithm is unaffected by daily variations in noise level at the array, that is expected to be particularly evident on islands (Fig. 2a) where meteorological weather can change rapidly. In order to trigger the alert, the *IP* has to exceed the threshold value of 100 for at least 30 min (see Section 3.4) as well as the signal-to-noise ratio has to be high for that time interval. By using a 24-h latency time on the notification, even if the *IP* returns to sub-threshold values, the problem of day-scale noise level variations is avoided.

Comparing our work with others, the brute-force, grid-search, cross-bearings method of Matoza et al. (2017) needs volcanic infrasound being recorded at least by two stations in order to identify an eruptive explosive event and provide a notification. This increases the reliability of notifications at the expense of fewer events detected due to both IMS network coverage and infrasound seasonality (Morelli et al., 2022). Reliability increases through elimination of those repetitive and persistent sources of coherent infrasonic signals (clutter) through background prior rate correction in a global grid. In contrast, the monitoring approach presented in this study, exploits single array observations providing notifications on each ongoing phase of an entire eruptive cycle only with the back-azimuth of the infrasonic wave. The identification of the volcanic signal is based on the *IP* with the two additional thresholds with no other constraints on the source location. However, the range corrected pressure (p_s), calculated assuming the real distance between the volcano and the receiver (e.g. 1150 km for the Anak-Krakatau), is implicitly constraining the source location.

According to Eq. (5), the pressure at the source will be overestimated in case the signal is produced by a source closer to the array with the same back-azimuth of the volcano. Therefore, the attenuation coefficient of the closer source must be significantly smaller than the A_P calculated from Eq. (2) considering the real volcano-to-receiver distance. As a result, retrieved range-corrected pressure amplitudes will likely be too large for volcanic explosive eruptions. Indeed, infrasound observations performed at local distances suggest that maximum pressure at the reference distance of 1 km from the source is generally not exceeding few hundreds of Pascal (Fee and Matoza, 2013). This consideration does not hold for highly explosive volcanic eruptions, like the recent January, 15, 2022 eruption of Hunga volcano (Matoza et al., 2022; Vergoz et al., 2022), that produced an explosive shock wave exceeding 100 Pa at a distance of 1847 km (Vergoz et al., 2022). Moreover, pressures above 500 Pa are representative of short-impulsive infrasonic transients associated with the initial stages of an eruptive event (e.g., conduit clogging or new magma input), sometimes followed by more sustained with a moderate amplitude activity (Fee and Matoza, 2013). In this case, the proposed method will be able to notify the event with a delay due to high-amplitude phase exclusion.

Therefore the additional threshold proposed for the range corrected pressure ($p_s < 500Pa$), that represents a constraint on the source-to-receiver distance, allows to reduce the ambiguity of signal identification without significantly reducing the applicability of the method.

The experimental threshold on 33% of the signal persistency, that we proposed based on multi-year observation of infrasound data from IS06 IMS array, is a critical parameter to minimize false alerts, but, at the same time, it is limiting the applicability of this approach to high intensity, long-lasting events, such as Sub-Plinian or Plinian eruptions. Although both discrete, short-lasting Vulcanian explosions or long lasting VEI 3 (and more) eruptions are able to drive thermal plumes reaching altitudes of 10 km or more, their impact is very different. As a matter of the fact, long lasting events are able to produce a minimum 0.01 km^3 of pyroclastic material, like blocks, bombs, and especially ash, thus resulting in a larger ash plume extension and, consequently, dispersion. It is clear that sustained eruptions, that are driving long-lasting atmospheric perturbations (Garcés et al., 2008; Ripepe et al., 2010; Fee and Matoza, 2013), are of greater interest to aviation rather than single thermals.

If we consider a short-lasting infrasonic transient, the signal duration increases with source-to-receiver distance, due to the increased separation of the fastest and slowest portions of the wave-field propagating within atmospheric acoustic waveguides (Green and Nippress, 2019), and might last up to ~ 6 minutes for a source to receiver distance of 1000 km. Considering the time window of analysis $W = 20$ min proposed here, this duration might result in a maximum of number of detections N_{det} of 30. Hence, we suggest to consider only signals with significant persistency (N_{det} >33) in *IP* calculation, in order to consider only sustained events and reduce the number of false alerts (Fig. 5c).

Results presented in this study show that the application of the additional thresholds to the *IP* allows to minimize false alerts but limits the proposed analysis to detect and notify major,long lasting, explosive eruptions, while leaving smaller scale short-lasting explosive events undetected (Fig. 6). Indeed, while the 2018 Anak-Krakatau and the 2014 Kelut volcano explosive eruptions cause a significant increase in *IP* and are therefore notified, lower intensity explosive events are not detected. Sinabung volcano represents the only exception in our analysis, due to the lack of notifications for its 2018–2019 high eruption intensity (VEI 4). As a matter of fact, According to GVP reports, Sinabung volcano produced long lasting eruptions with high plumes (~ 15 km a.s.l) both in February 2018 and in May and June 2019, but its *IP* was not significantly increased (Fig. 6) during the 8 years of analysis. The lack of significant infrasonic signals recorded by the array and produced by Sinabung eruption can be attributed to the unfavorable propagation conditions, that persisted during the whole period of analysis.

As described in Section 3.2, the $V_{eff-ratio}$ controls the refraction of energy in the stratopause region towards the ground and it is strongly dependent on the stratospheric wind direction. When $V_{eff-ratio}$ is below 1, the attenuation of the signal is strong and may cause the total dissipation of energy (Pichon et al., 2012). As visible in Fig. 6, the

attenuation retrieved from $V_{eff-ratio}$ for each volcano is strongly affected by the stratospheric zonal winds that blow from East to West in Austral summer and West to East in Austral winter. For this reason, infrasound propagation for signals produced from volcanoes that are located to the East or to the West from the array, is affected by a strong seasonal attenuation from a minimum of −50 dB to a maximum of −100 dB. On the contrary, propagation of infrasound produced by volcanoes located along the North–South direction with respect to the array, is more or less constant through time and is controlled by the source to receiver distance. For the specific case of Sinabung volcano, that is located North of the station (back-azimuth 5°) at a distance of 1720 km to the array, we expect an attenuation spanning between −65 and −75 dB, which likely prevents the infrasound radiated by the volcano from being recorded at the array.

From Fig. 6, it is clear that volcanoes with similar back-azimuth with respect to the station will show similar *IP* trends and this might lead to multiple alerts from adjacent volcanoes triggered by explosive eruptive activity occurring at one volcano only. This is a direct consequence of the azimuthal deviation Δaz_V considered for extracting the detections used to calculate *IP*. Certainly, the use of multiple arrays would help source identification by decreasing the ambiguity imposed by the different infrasound source types and especially to ignore persistent infrasound sources close to the source as sources of possible false alarms. Rose and Matoza (2021) apply this approach to the 2018 Anak-Krakatau eruption by cross-referencing data from multiple stations including IS06 and IS52 at 3638 km. However, the back-azimuth intersection with both arrays identifies a point 128 km away from the actual source. Moreover a similar problem was already encountered by Matoza et al. (2017), where the grid search method does often not reach a resolution that identifies a single source due to azimuthal ray deviation.

It is impossible to solve completely the ambiguity and superimposition related to volcanoes with a similar back-azimuth to one array. However, in a long range, global monitoring perspective, this limitation might be reduced when considering volcanic sectors rather than single volcanoes. Fig. 7a represents a possible solution for the 64 active volcanoes of the Indonesian Volcanic arc that had activity during the Holocene and are positioned within 2000 km from IS06 array. Volcanoes are grouped into nine distinct, separate azimuthal intervals, even considering the applied azimuthal deviation Δaz_V of ±3° could be identified by the array without any superposition and ambiguity. By applying the *IP* calculation to infrasound detections with a back-azimuth consistent with the various azimuthal intervals covering the whole Indonesian Arc within the distance of 2000 km from the array (Fig. 7), we obtain a highly reliable detection of volcanic activity from specific sectors without issuing any false alerts. Fig. 7 shows how the system is able to identify the activity in sector VII and sector IX due to the occurrence of Anak-Krakatau and Kelut eruptive phases respectively. In the other sectors any notifications are triggered in agreement with the results on individual volcanic edifices. The notification of activity within a given sector might be a valuable information to the VAACs to pay more attention to the area. This implementation will be very useful and probably necessary when the method is applied to other IMS stations characterized by a dense distribution of active volcanoes around the array (e.g. IS44, Kamchatka Peninsula).

Some additional approaches (beyond the scope of this study) could be investigated to reduce the ambiguity of detections and to extract more information about volcano sources. Future progress could concern the azimuthal deviation's correction. In this study we assume that the long range detected infrasonic waves propagate within the stratospheric waveguides (Sections 3.1 and 3.2), where deflection due to the strong east–west winds is severe (Pichon et al., 2005), especially for infrasonic rays traveling in the north–south direction (e.g Sinabung). The azimuth

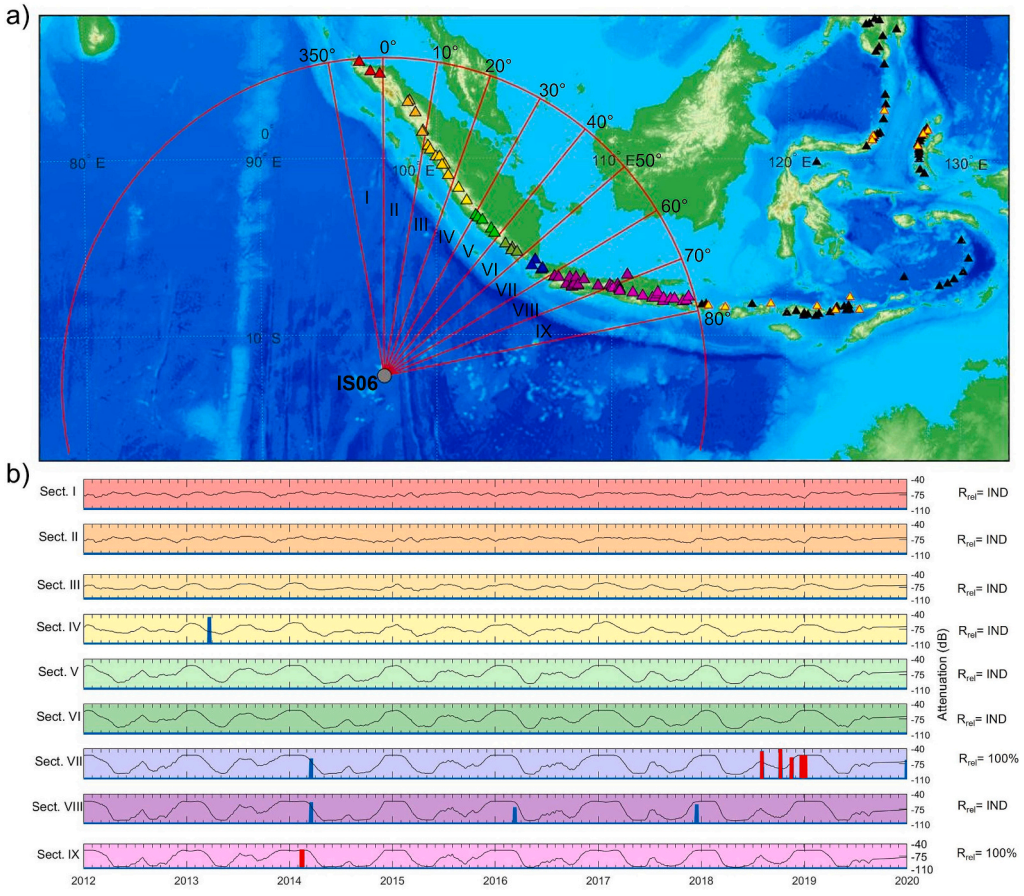

Fig. 7. a),The nine sectors that grouped the 64 volcanoes within a source-to-receiver distance <2000 km from the IS06 IMS infrasound array (grey dot). The sectors are identified taking into account for azimuth deviation Δaz_V of each volcano. The sectors are 10° wide and cover the entire distribution of the volcanoes identified by the station. The different colors belong to different sectors. In b), the *IP* (blue lines, while in red when notifications are expected) and the Reliability ratio for the nine sectors are depicted. *IP* is calculated as described in Section 3 considering a mean distance and attenuation between IS06 and volcanoes belonging to each sector.The black line is the attenuation along the source-to-receiver path, see Section 3.2.

deviation is induced by this wind effects and could be corrected using ray tracing from the source to the receiver.

Another point would be the calculation of the attenuation of detections. It is a critical parameter to filter out false alarms and extract information and characteristics on ongoing volcanic activity. Complete waveform modeling tools bring reliable estimation of source parameters but have extensive computational costs that prevent their use in operational applications. Current research in this field includes artificial intelligence and models that, once trained, could generate the waveform in seconds (Brissaud and Astafyeva, 2022), allowing us to compute the attenuation in real time.

Finally, ash cloud height's estimation from acoustic pressure at the source is still an open topic (De Angelis et al., 2019; Diaz-Moreno et al., 2019) but further research could provide more information about the source inferred from infrasound signals. This parameter, used as an input parameter for ash dispersion models, could help predict ash cloud transport in the airspace.

6. Conclusions

Many volcanoes worldwide are poorly monitored or still unmonitored. Most of the time, for poorly monitored volcanoes, information concerning ongoing volcanic activity is provided by satellite imagery only or by pilot reports after (sometimes many hours) the event started (Lechner et al., 2017), thus resulting in a possible delay in the issuance of Volcanic Ash Advisories (VAAs). In order to compensate for the lack of observations and to give a fast notification to the VAACs, the IMS infrasound array network offers the possibility to conduct regional-to-global scale volcano monitoring. Previous studies (Matoza et al., 2017; Marchetti et al., 2019; Pichon et al., 2021) demonstrated that infrasound detections have appeared as an additional mean to collect timely data on the eruptions even at long source-to-receiver range, but an analysis on the efficiency and on the rate of false alerts is still missing.

In this study we propose a single array method to monitor volcanoes at long (200–2000 km) range with the Infrasound Parameter (*IP*), a detection algorithm based on the signal persistency (N_{det}) and on the acoustic amplitude corrected for propagation (p_s). We focus our analysis on 8 years of infrasound data recorded by the IS06 IMS station (Cocos Island, Australia), targeting active Indonesian volcanoes during the period of analysis and located within 2000 km from the array. Differently from previous studies we introduce two additional thresholds based on signal persistency ($N_{det} > 33$) and range corrected infrasound amplitude ($p_s < 500$ Pa). Resulting notifications are, eventually, compared with the GVP reports to quantify the false alerts and estimate the Reliability ratio (R_{rel}) for each Indonesian volcano, in order to validate the whole procedure.

Our approach identifies, without false alerts (R_{rel}=100), the 2018, VEI 3, eruption of Anak-Krakatau volcano, detecting not only the main event on 22 December but also portions of the preliminary high intense Strombolian and Vulcanian explosions, as well as the 2014, VEI 4, eruption of Kelut volcano. Differently, the 2018–2019 activity of Sinabung volcano was undetected, likely due to the unfavorable propagation conditions that prevented significant infrasound to be recorded at the source-to-receiver distance of 1720 km; hence *IP* remained at low values without triggering any notification. The other eight Indonesian volcanoes (i.e. Marapi, Kerinci, Dempo, Slamet, Merapi, Tengger Caldera, Semeru and Raung volcanoes) that were active during the period of analysis (i.e., 2012–2019) did not produced high-intense explosive volcanic eruptions, and potentially radiated infrasound was not recorded at the array due to low intensity at the source and/or unfavorable propagation conditions. At the same time, no false alerts have been recorded either (R_{rel}=IND), thus suggesting that in case of a major, long lasting explosive eruption, radiated infrasound might be detected by the array during favorable propagation conditions and a reliable notification possibly delivered. Moreover, considering a travel time from source to receiver distance of 1000 km is 50 min (assuming a celerity of 310–330 m/s), this could be the faster approach to obtain observations on ongoing volcanic activity compare to the return periods of 12 h of NASA satellites (Carr et al., 2016).

The presented results clearly show, however, that the detection and notification procedure presented here is limited by infrasound propagation conditions and by overlapping of infrasound back-azimuth of different volcanoes to the array (e.g. Kelut, Tengger Caldera and Semeru volcanoes). The infrasound ray tracing should be a possible solution to reduce the azimuth deviation and obtain accurate identification of detections. However, this latter effect might be reduced by grouping active volcanoes around the array into distinct azimuthal sectors, that despite preventing the notification of ongoing activity at a given volcano might drive the attention of the VAACs to specific areas.

Based on the presented results, we conclude that our approach might allow to deliver a notification from IS06 infrasound array data, in near real-time, of major (>VEI 3) ongoing volcanic activity during favorable propagation conditions (Austral summer) within any volcanic sector of the Indonesian arc with high reliability and without false alerts. This implementation will be very useful and probably necessary when the method is applied to other IMS stations characterized by a dense distribution of active volcanoes around the array (e.g. I44RU in Kamchatka peninsula). In this way, by applying this approach to other IMS stations, we will be able to refine and set up a general procedure to investigate volcanic activity at global scale and estimate the global reliability of the IMS infrasound network in this context.

CRediT authorship contribution statement

Duccio Gheri: Writing-original-draft, Conceptualization, Data-curation, Supervision, Validation, Methodology, Software, Writing-review-editing. **Emanuele Marchetti:** Writing-original-draft, Conceptualization, Supervision, Validation, Methodology. **Giacomo Belli:** Conceptualization, Supervision, Validation, Methodology. **Alexis Le Pichon:** Supervision, Validation, Methodology. **Vincent Boulenger:** Validation, Methodology. **Patrick Hupe:** Data-curation, Validation. **Lars Ceranna:** Supervision. **Pierrick Mialle:** Supervision, Data-curation. **Philippe Hereil:** Supervision.

Declaration of Competing Interest

The authors declare that they have no known competing financial interests or personal relationships that could have appeared to influence the work reported in this paper.

Data availability

The data that has been used is confidential.

Acknowledgments

The views expressed herein are those of the authors and not necessarily reflect the views of the CTBTO Preparatory Commission. The authors are grateful to the CTBTO and IMS station operators for guaranteeing the high-quality infrasound data, acknowledges the CTBTO Preparatory Commission for providing limited access (via vDEC) to the IMS infrasound network data.This study was facilitated by previous research performed within the framework of the ARISE project, funded by the European Commission FP7 and Horizon 2020 programs (Grant agreements 284387 and 653980). The University of Florence acknowledges the contribution of the National Recovery and Resilience Plan, Mission 4 Component 2 - Investment 1.4 - NATIONAL CENTER FOR HPC, BIG DATA AND QUANTUM COMPUTING - funded by the European Union - NextGenerationEU - CUPB83C22002830001.

References

Bowman, J.R., Baker, G.E., Bahavar, M., 2005. Ambient infrasound noise. Geophys. Res. Lett. 32 (9).

Brissaud, Q., Astafyeva, E., 2022. Near-real-time detection of co-seismic ionospheric disturbances using machine learning. Geophys. J. Int. 230 (3), 2117–2130.

Cansi, Y., 1995. An automatic seismic event processing for detection and location: The pmcc method. Geophys. Res. Lett. 22 (9), 1021–1024.

Carr, B.B., Clarke, A.B., Vanderkluysen, L., 2016. The 2006 lava dome eruption of merapi volcano (indonesia): Detailed analysis using modis tir. J. Volcanol. Geoth. Res. 311, 60–71.

Casadevall, T.J., 1994. The 1989–1990 eruption of redoubt volcano, alaska: impacts on aircraft operations. J. Volcanol. Geoth. Res. 62 (1–4), 301–316.

Caudron, C., Taisne, B., Garcés, M., Alexis, L.P., Mialle, P., 2015. On the use of remote infrasound and seismic stations to constrain the eruptive sequence and intensity for the 2014 kelud eruption. Geophys. Res. Lett. 42 (16), 6614–6621.

Christie, D., Campus, P., 2010. The ims infrasound network: Design and establishment of infrasound stations. In: Infrasound monitoring for atmospheric studies. Springer, pp. 29–75.

Dabrowa, A., Green, D., Rust, A., Phillips, J., 2011. A global study of volcanic infrasound characteristics and the potential for long-range monitoring. Earth Planet. Sci. Lett. 310 (3–4), 369–379.

De Angelis, S., Diaz-Moreno, A., Zuccarello, L., 2019. Recent developments and applications of acoustic infrasound to monitor volcanic emissions. Remote Sens. 11 (11), 1302.

De Angelis, S., Fee, D., Haney, M., Schneider, D., 2012. Detecting hidden volcanic explosions from mt. cleveland volcano, alaska with infrasound and ground-coupled airwaves. Geophys. Res. Lett. 39 (21).

Diaz-Moreno, A., Iezzi, A., Lamb, O., Fee, D., Kim, K., Zuccarello, L., De Angelis, S., 2019. Volume flow rate estimation for small explosions at mt. etna, italy, from acoustic waveform inversion. Geophys. Res. Lett. 46 (20), 11071–11079.

Drob, D.P., Picone, J., Garcés, M., 2003. Global morphology of infrasound propagation. J. Geophys. Res.: Atmos. 108 (D21).

Engwell, S., Mastin, L., Tupper, A., Kibler, J., Acethorp, P., Lord, G., Filgueira, R., 2021. Near-real-time volcanic cloud monitoring: insights into global explosive volcanic eruptive activity through analysis of volcanic ash advisories. Bull. Volcanol. 83 (2), 1–17.

Evans, J.E., 1994. Development of a real-time atc volcanic ash advisory system based on the future aviation weather system. In: Volcanic ash and aviation safety: Proceedings of the First International Symposium on Volcanic Ash and Aviation Safety. US Geological Survey Bulletin 2047, pp. 157–31.

Fee, D., Garces, M., Steffke, A., 2010. Infrasound from tungurahua volcano 2006–2008: Strombolian to plinian eruptive activity. J. Volcanol. Geoth. Res. 193 (1–2), 67–81.

Fee, D., Matoza, R.S., 2013. An overview of volcano infrasound: From hawaiian to plinian, local to global. J. Volcanol. Geoth. Res. 249, 123–139.

Garcés, M., Fee, D., Steffke, A., McCormack, D., Servranckx, R., Bass, H., Hetzer, C., Hedlin, M., Matoza, R., Yepes, H., et al., 2008. Capturing the acoustic fingerprint of stratospheric ash injection. Eos, Trans. Am. Geophys. Union 89 (40), 377–378.

Gössling, S., Humpe, A., 2020. The global scale, distribution and growth of aviation: Implications for climate change. Global Environ. Change 65, 102194.

Green, D.N., Nippress, A., 2019. Infrasound signal duration: The effects of propagation distance and waveguide structure. Geophys. J. Int. 216 (3), 1974–1988.

Grilli, S.T., Tappin, D.R., Carey, S., Watt, S.F., Ward, S.N., Grilli, A.R., Engwell, S.L., Zhang, C., Kirby, J.T., Schambach, L., et al., 2019. Modelling of the tsunami from the december 22, 2018 lateral collapse of anak krakatau volcano in the sunda straits, indonesia. Sci. Rep. 9 (1), 1–13.

Guffanti, M., Casadevall, T.J., Budding, K.E., 2010. Encounters of aircraft with volcanic ash clouds: A compilation of known incidents, 1953–2009. US Department of Interior, US Geological Survey.

Gunawan, H., Budianto, A., Prambada, O., McCausland, W., Pallister, J., Iguchi, M., et al., 2019. Overview of the eruptions of sinabung volcano, 2010 and 2013–present and details of the 2013 phreatomagmatic phase. J. Volcanol. Geoth. Res. 382, 103–119.

ICAO, 2019. Future of aviation. Available:// https://www.icao.int/Meetings/FutureOfAviation/Pages/default.aspx.

Johnson, J.B., Ripepe, M., 2011. Volcano infrasound: A review. J. Volcanol. Geoth. Res. 206 (3–4), 61–69.

Kalinowski, M.B., Mialle, P., 2021. Introduction to the topical issue on nuclear explosion monitoring and verification: Scientific and technological advances. Pure Appl. Geophys. 178 (7), 2397–2401.

Kristiansen, N.I., Prata, A., Stohl, A., Carn, S.A., 2015. Stratospheric volcanic ash emissions from the 13 february 2014 kelut eruption. Geophys. Res. Lett. 42 (2), 588–596.

Le Pichon, A., Blanc, E., Drob, D., Lambotte, S., Dessa, J., Lardy, M., Bani, P., Vergniolle, S., 2005. Infrasound monitoring of volcanoes to probe high-altitude winds. J. Geophys. Res.: Atmos. 110 (D13).

Le Pichon, A., Ceranna, L., Vergoz, J., 2012. Incorporating numerical modeling into estimates of the detection capability of the ims infrasound network. J. Geophys. Res.: Atmos. 117 (D5).

Le Pichon, A., Pilger, C., Ceranna, L., Marchetti, E., Lacanna, G., Souty, V., Vergoz, J., Listowski, C., Hernandez, B., Mazet-Roux, G., et al., 2021. Using dense seismo-acoustic network to provide timely warning of the 2019 paroxysmal stromboli eruptions. Sci. Rep. 11 (1), 1–12.

Le Pichon, A., Vergoz, J., Blanc, E., Guilbert, J., Ceranna, L., Evers, L., Brachet, N., 2009. Assessing the performance of the international monitoring system's infrasound network: Geographical coverage and temporal variabilities. J. Geophys. Res.: Atmos. 114 (D8).

Lechner, P., Tupper, A., Guffanti, M., Loughlin, S., Casadevall, T., 2017. Volcanic ash and aviation—the challenges of real-time, global communication of a natural hazard. In: Observing the volcano world. Springer, pp. 51–64.

Marchetti, E., Ripepe, M., Campus, P., Le Pichon, A., Vergoz, J., Lacanna, G., Mialle, P., Hereil, P., Husson, P., 2019. Long range infrasound monitoring of etna volcano. Sci. Rep. 9 (1), 1–10.

Marty, J., 2019. The ims infrasound network: current status and technological developments. In: Infrasound monitoring for atmospheric studies. Springer, pp. 3–62.

Marty, J., Denis, S., Gabrielson, T., Garcés, M., Brown, D., 2017. Comparison and validation of acoustic response models for wind noise reduction pipe arrays. J. Atmos. Ocean. Technol. 34 (2), 401–414.

Matoza, R.S., Fee, D., Assink, J.D., Iezzi, A.M., Green, D.N., Kim, K., Toney, L., Lecocq, T., Krishnamoorthy, S., Lalande, J.-M., et al., 2022. Atmospheric waves and global seismoacoustic observations of the january 2022 hunga eruption, tonga. Science.

Matoza, R.S., Green, D.N., Le Pichon, A., Shearer, P.M., Fee, D., Mialle, P., Ceranna, L., 2017. Automated detection and cataloging of global explosive volcanism using the international monitoring system infrasound network. J. Geophys. Res.: Solid Earth 122 (4), 2946–2971.

Matoza, R.S., Vergoz, J., Le Pichon, A., Ceranna, L., Green, D.N., Evers, L.G., Ripepe, M., Campus, P., Liszka, L., Kvaerna, T., et al., 2011. Long-range acoustic observations of the eyjafjallajökull eruption, iceland, april–may 2010. Geophys. Res. Lett. 38 (6).

Morelli, R.S., Gheri, D., Campus, P., Coppola, D., Marchetti, E., 2022. Long range infrasound monitoring of yasur volcano. J. Volcanol. Geoth. Res. 432, 107707.

Newhall, C.G., Self, S., 1982. The volcanic explosivity index (vei) an estimate of explosive magnitude for historical volcanism. J. Geophys. Res.: Oceans 87 (C2), 1231–1238.

Perttu, A., Caudron, C., Assink, J., Metz, D., Tailpied, D., Perttu, B., Hibert, C., Nurfiani, D., Pilger, C., Muzli, M., et al., 2020. Reconstruction of the 2018 tsunamigenic flank collapse and eruptive activity at anak krakatau based on eyewitness reports, seismo-acoustic and satellite observations. Earth Planet. Sci. Lett. 541, 116268.

Ripepe, M., De Angelis, S., Lacanna, G., Voight, B., 2010. Observation of infrasonic and gravity waves at soufrière hills volcano, montserrat. Geophys. Res. Lett. 37 (19).

Ripepe, M., Marchetti, E., Delle Donne, D., Genco, R., Innocenti, L., Lacanna, G., Valade, S., 2018. Infrasonic early warning system for explosive eruptions. J. Geophys. Res.: Solid Earth 123 (11), 9570–9585.

Rose, K.M., Matoza, R.S., 2021. Remote hydroacoustic-infrasonic detection and characterization of anak krakatau eruptive activity leading to, during, and following the december 2018 flank collapse and tsunami. Bull. Volcanol. 83 (8), 1–17.

Ulivieri, G., Ripepe, M., Marchetti, E., 2013. Infrasound reveals transition to oscillatory discharge regime during lava fountaining: Implication for early warning. Geophys. Res. Lett. 40 (12), 3008–3013.

Venzke, E.e., 2013. Volcanoes of the world, v4.10.3 (15 Oct 2021). Smithsonian Institution.

Vergoz, J., Hupe, P., Listowski, C., Le Pichon, A., Garcés, M., Marchetti, E., Labazuy, P., Ceranna, L., Pilger, C., Gaebler, P., et al., 2022. Ims observations of infrasound and acoustic-gravity waves produced by the january 2022 volcanic eruption of hunga, tonga: A global analysis. Earth Planet. Sci. Lett. 591, 117639.

Walter, T.R., Haghshenas Haghighi, M., Schneider, F.M., Coppola, D., Motagh, M., Saul, J., Babeyko, A., Dahm, T., Troll, V.R., Tilmann, F., et al., 2019. Complex hazard cascade culminating in the anak krakatau sector collapse. Nat. Commun. 10 (1), 1–11.

Webley, P., Mastin, L., 2009. Improved prediction and tracking of volcanic ash clouds. J. Volcanol. Geoth. Res. 186 (1–2), 1–9.

Ye, L., Kanamori, H., Rivera, L., Lay, T., Zhou, Y., Sianipar, D., Satake, K., 2020. The 22 december 2018 tsunami from flank collapse of anak krakatau volcano during eruption. Sci. Adv. 6 (3), eaaz1377.